Coastal Engineering Journal, Vol. 43, No. 1 (2001) 39–58

WATER WAVE INTERACTION OF TWIN LARGE SCALE CAISSONS WITH A SMALL GAP BETWEEN

GUOPING MIAO
School of Naval Architecture and Ocean Engineering, Shanghai Jiao Tong University, Shanghai 200030, China

TAKEHISA SAITOH* and HAJIME ISHIDA
Department of Civil Engineering, Kanazawa University, 2-40-20 Kodatsuno, Kanazawa 920-8667, Japan

Received 11 November 1999
Revised 1 December 2000

A reduced two-dimensional source distribution method is used for systematic computations on wave interaction of twin vertical cylinders with rectangular sections aligned with small gap between in order to get a clear fundamental view of small gap influence to the force response on potential very large coastal and marine structures. Strong hydrodynamic interaction between caissons with small gap is observed and sharp peak force responses are proved in the paper by both numerical evidence and theoretical verification due to newly discovered narrow open channel resonant phenomena. This strong interaction feature has its own important practical significance for design of links of modules for the large structure and attentions on terms of work for linking the modules. And moreover, the importance is also closely related to hydro-elasticity analyses for the very large structures, in which local loads may be as important as integrated loads.

Keywords: Wave-structure interaction, twin caissons with small gap, narrow open channel resonance, very large coastal and marine structures.

1. Introduction

Recently, investigation on very large coastal and marine structures has aroused large interests in coastal and ocean engineering around the world due to their important potential usage. For example, so-called very large floating structures (Kagemoto *et al.*, 1997) denote those floating structures with dimension scale of kilometers and are by this feature distinguished from the conventional large ships and ocean platforms with dimension scale of several hundred meters. We, moreover, can find many plans for an effective using of coastal and ocean area by constructing very large structures.

Since the very large coastal and marine structure may be composed of large amount of modules (unit blocks) in fact, there will be many gaps between them,

*E-mail: saitoh@t.kanazawa-u.ac.jp

which should be small by comparing with the characteristic dimension of the modules. In addition to this, during the construction of the structures, we cannot avoid a term of work for linking the modules, in which each module's extreme vicinity happens.

Comprehensive studies on multi-body interaction, however, are mostly limited to cases with larger separation distances between bodies up to now. For example, in regard to floating bodies, Ohkusu (1976) and Oortmerssen (1979) investigated hydrodynamic interaction between two floating bodies, and showed that interaction effects in the hydrodynamic reaction forces could be quite significant. But the distance between two floating bodies exceeded half of the typical length of the floating bodies. On the other hand, in regard to bottom mounted cylinders, Linton and Evans (1990) and Kim (1993) investigated wave scattering interaction with an array of circular cylinders in a open sea. Kiyokawa and Motyka (1990) developed an analytical method for the infinite periodic row of cylinders with arbitrary cross sections. Dalrymple and Martin (1990), Nakamura (1994) investigated wave directional change due to an array of breakwaters. Fernyhough and Evans (1995) and Nakamura (1997) attempted to calculate in the case of a periodic array of rectangular blocks. Moreover, for the circular cylinders arbitrarily spaced along a centerline of a wave channel, Evans and Porter (1997) pointed out trapped mode interaction which strongly depended on the specified relationship between the wave number and the channel width. But the distances between the cylinders, the cylinder and the channel wall were not so narrow.

It seems, therefore, that we still lack of knowledge about the influence of small gaps due to each body's further vicinity on the wave loading on the structures and the interaction between them. The present study seems to look at the first attempt aimed to give an insight into that matter of gap influence on the wave forces and multi-body interactions.

If the gap influence could be verified small enough to be neglected for the very large structures with small gaps, it would be safe to use an integrated single body approximation. If the situation is on the contrary, however, some special attention should be made to take the gap influence into account efficiently, including the term of work for linking the modules. We may need to find some simplified ways to overcome the difficulty appeared in using the boundary element method to treat the hydrodynamic problems for the very large structures with extremely large amount of unit modules and gaps.

As a first step aiming to judge the gap influence to the multi-body hydrodynamic interaction, twin bottom mounted vertical cylinders with rectangular sections aligned with small gap between will be mostly concern in the paper. Several reasons can be listed for the choice of the present simplified model. For such special body configurations, a reduced two-dimensional source distribution method can be utilized for systematic computations with various parameter combinations. Isaacson (1978) among others developed this method for wave forces on a single cylinder of

arbitrary section. And later on it was further extended by Miao *et al.* (1993, 1998) for both the wave forces and hydrodynamic forces on vibrating cylinders and for multiple cylinder interactions. Moreover, it is believed that the hydrodynamic interaction between such bottom mounted rectangular caissons would be much stronger and clearer to be noticed than that, for example, between floating box-shaped bodies. There is no principal difficulty to account for hydrodynamic interactions for more caissons, however, the results for more bodies can be understood and explained in a correct way only when we have had a clear view on the two caissons interaction.

Indeed, in the present study, a strong hydrodynamic interaction between caissons is observed and the sharp peak force on each caisson may reach ten times the value for the same but well separated caissons or isolated caisson at some special frequencies. The sharp force responses are proved in the paper due to the newly discovered narrow open channel resonant phenomena by both numerical evidence and theoretical verification. The strong hydrodynamic interaction feature has its own important practical significance for the design of links (connectors) of modules for the very large structures and the attentions on the term of work for linking the modules. And moreover, the importance is also closely related to the hydro-elasticity analyses for the very large coastal and marine structures, in which local loads may be as important as the integrated loads.

2. Formulation and Solution of the Problem

Although the following formulation and solution procedure are generally valid for any number of vertical cylinders in waves, we limit our discussions in the paper to twin vertical cylinders with rectangular section, which is referred to as twin caissons hereinafter for simplicity. Since the procedure is well-made and verified, only the outline of the procedure will be given for brevity. One may refer to Miao and Liu (1990) for more details in numerical treatment.

Suppose we have two aligned caissons of rectangular section in waters of constant depth h with one end mounted on the sea bottom and the other piercing the free surface. Both of the caissons are identical with length of L and breadth of B, $B \leqq L$. There is a small uniform gap of width $2a$ between them, comparing with the main dimension of the caisson, i.e. $2a \ll B$. As shown in Fig. 1, a Cartesian coordinate system $oxyz$ is defined with the origin on the undisturbed free surface and oz axis pointing vertically upward. The relative position of oz axis to the caissons is not quite significant. For the convenience of later description, we locate it going through the middle point of the gap at the right-hand side. The ox axis is along the gap pointing positively out of caissons and the oy axis is then on one of the side-walls of caissons. The regular incident wave propagates with an incident angle of α to the positive ox axis.

We treat the problem in the linear potential theory regime in the frequency domain. The fluid motion can be described by the velocity potential $\Phi(x, y, z, t) =$

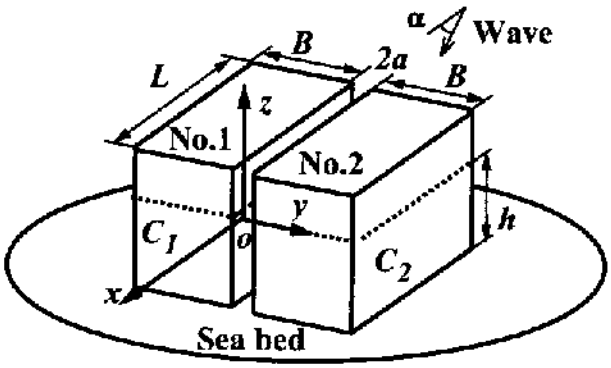

Fig. 1. Twin caissons and the coordinate system.

$\phi(x,y,z)e^{-i\omega t}$ under the usual assumption of ideal and incompressible fluid and irrotational flow for time-harmonic motions of frequency ω. The spatial potential $\phi(x,y,z)$ can be regarded as the superposition of the incident wave potential $\hat{\phi}_I(x,y,z)$ and the diffraction potential $\hat{\phi}_D(x,y,z)$.

It is well known that the incident wave potential in finite water depth can be expressed as

$$\hat{\phi}_I(x,y,z) = \phi_I(x,y)\frac{\cosh k(z+h)}{\cosh kh} \tag{1}$$

$$\phi_I(x,y) = \bar{A}e^{ik(x\cos\alpha + y\sin\alpha)}, \qquad \bar{A} = -\frac{igA}{\omega} \tag{2}$$

where A is the wave amplitude, α represents the incident wave angle with respect to the ox axis, and k is the wave number governed by the dispersion relation

$$\omega^2 = gk\tanh kh\,. \tag{3}$$

Due to the present special body configuration, the diffraction potential $\hat{\phi}_D(x,y,z)$ may also be correspondingly written as

$$\hat{\phi}_D(x,y,z) = \phi_D(x,y)\frac{\cosh k(z+h)}{\cosh kh} \tag{4}$$

with z dependence separated and free surface and bottom boundary conditions satisfied. The boundary value problem for $\phi_D(x,y)$ is then reduced to two-dimensional and formed by the two-dimensional Helmholtz equation and corresponding boundary conditions as follows, i.e.

$$\frac{\partial^2\phi_D}{\partial x^2} + \frac{\partial^2\phi_D}{\partial y^2} + k^2\phi_D = 0 \qquad \text{in the fluid domain} \tag{5}$$

$$\frac{\partial\phi_D}{\partial n} = -\frac{\partial\phi_I}{\partial n} \qquad \text{on the body surface} \tag{6}$$

$$\lim_{r\to\infty}\sqrt{r}\left(\frac{\partial\phi_D}{\partial r}-ik\phi_D\right)=0 \tag{7}$$

where $\partial/\partial n$ is the derivative operator along the inner-pointing unit normal vector of the body surface. ϕ_D may be represented by the source and sink distribution method as

$$\phi_D(P)=\frac{1}{4\pi}\int_C \sigma(Q)G(P,Q)dl \tag{8}$$

where C denotes the sectional girth of all the bodies ($C=C_1+C_2$), and

$$G(P,Q)=i\pi H_0^{(1)}(kr) \tag{9}$$

is the fundamental source solution of Eq. (5), in which $P(x,y)$ and $Q(\xi,\eta)$ denote the field point and source point, respectively, and $r=[(x-\xi)^2+(y-\eta)^2]^{1/2}$ is the distance between them. $H_0^{(1)}(kr)$ is the first kind Hankel function of the zero-th order having $\ln r$ type singularity as $r\to 0$ and satisfying the radiation condition of out-going disturbance waves (7) as $r\to\infty$. $\sigma(Q)$ is the source distribution strength being determined by imposing the body surface condition (6) to form a Fredholm integral equation of the second kind

$$\frac{1}{2}\sigma(P)+\frac{1}{4\pi}\int_C \sigma(Q)\frac{\partial G(P,Q)}{\partial n}dl=-\frac{\partial\phi_I(P)}{\partial n}. \tag{10}$$

The integral equation can be solved by discretization technique. The body sectional girth C may be divided and approximated into N linear segments. The source distribution strength $\sigma(Q)$ is assumed constant on each segment and the integral equation is satisfied at the middle of each segment. Equation (10) is then discretized into a set of N linear algebraic equations with N unknown source distribution strengths, i.e.

$$\sum_{j=1}^{N}E_{ij}\sigma_j=-\frac{\partial\phi_I(P_i)}{\partial n},\qquad i=1,2,\ldots,N \tag{11}$$

or in matrix form as

$$[E]\{\sigma\}=\{F\} \tag{12}$$

where

$$E_{ij}=\begin{cases}\dfrac{1}{2} & i=j\\[2ex] \dfrac{1}{4\pi}\displaystyle\int_{\Delta C_i}\frac{\partial G(P_i,Q_j)}{\partial n}dl & i\neq j\end{cases} \tag{13}$$

and $\{F\}$ has its elements shown as the right-hand term of Eq. (10). The source strength $\sigma(Q)$ is easy to obtain, i.e.

$$\{\sigma\}=[E^{-1}]\{F\} \tag{14}$$

Once the source strength $\sigma(Q)$ is solved, the velocity potential at any point P in the fluid domain can be determined by the discretized form of Eq. (8), which may also be written in a matrix expression as

$$\phi_D(P) = \{T\}^T\{\sigma\} \tag{15}$$

where

$$T_j = \frac{1}{4\pi}\int_{\Delta C_j} G(P,Q_j)dl \tag{16}$$

By the linearized Bernoulli's equation, the wave forces, including the Froude-krylov force and the diffraction force, exerted on the mth body can be obtained, i.e.

$$\mathbf{F}_m e^{-i\omega t} = e^{-i\omega t}\rho i\omega \int_{-h}^{0} dz \int_{C_m} \phi(P)\mathbf{n}dl \qquad \text{for } P \in C_m(m=1,2) \tag{17}$$

where $\mathbf{n}$ is the inner-pointing normal vector on the surface of the mth body.

As shown above the numerical modeling, the calculation has been directly done without any assumption for $2a \ll B$ in this numerical analysis.

3. Computational Results and Analysis

Systematic calculations for the wave forces on various twin caissons are carried out with the present method, which has been widely validated by comparison to the results for multi-bodies obtained by analytical solutions and the 3-D source distribution method (Miao and Liu, 1990, Miao *et al.*, 1993, 1998, Yu *et al.*, 1998). In order to exhibit the interesting interaction feature of twin caissons with small gap, the length of caissons L varies from 2 to 5 and the breadth B is kept constant as 2. It is implied that the linear scale of those caissons is made non-dimensional by the factor of $B/2$, as we always use the radius as a non-dimensional factor for the case of circular cylinders. For instance, the non-dimensional length of caissons could be written as $L/(B/2)$, and so for the wave length etc. For simplicity, however, we still use the original variables as non-dimensional ones later on without confusing. The width of the gap for all the calculation conditions is 0.02 (1% of the module breadth). For a real module with breadth of 60 m, the gap width would be 0.6 m. Gap width will surely give influence to the multi-body interaction features, which will be reported elsewhere later on.

In our calculations, each cylinder girth is divided into 40 segments to ensure the accuracy in shorter wave case. The non-dimensional wave number kL varies from 0.5 to 6.4, corresponding to the wavelength from $12.56L$ to $0.98L$ in the engineering interested range. Due to the sensitivity of the hydrodynamic interaction, the increment of kL is taken as small as 0.05 in order to detect the sharp resonant response as denoted below.

In the following figures, the horizontal axis represents the non-dimensional wave number kL, and the vertical axis represents the non-dimensional amplitude (modulus) of wave forces by the scale factor of $2\rho g A h D(\tanh kh/kh)$, where D indicates L and B according to the side length perpendicular to the wave force direction, respectively. This implies the results are transformed to the averaged wave force distribution in each force direction. The water depth h is taken as 10 in all the calculations, which actually gives no effects to the final results with the adopted non-dimensional factor for wave forces.

Shown in Figs. 2 and 3 are typical examples of the wave forces on each specified caisson with the length of 2 and 4 at wave incident angles $\alpha = 0°$ and 90°, respectively. In the case of $\alpha = 90°$, the caisson No. 1 denotes the leading one. As expected, only the in-line wave forces (the force in the same direction as waves) exist due to the symmetry when $\alpha = 90°$. And also due to the symmetry, the wave forces, including both in-line wave forces and cross wave direction forces, acting on either of twin caissons are the same when $\alpha = 0°$. The cross wave direction forces on each of the twin caissons are out of phase. In those figures, the results for corresponding isolated single caisson are also depicted for comparison, which may also be regarded as examples of the validation that the present method is free of the suffering of irregular frequencies in the frequency range we are interested in.

Sharp peak responses can be observed at some frequencies, which must relate to some resonant phenomena to which people seems not aware up to now. Indeed, this new resonant phenomenon can be proved to exist in the gap not only in the present numerical computations but also in the following theoretical verification, as given in the Appendix by extending the asymptotic matching process used by Mei (1989) for narrow harbor resonance. The resonant wave number can be proved around $kL = n\pi(n = 1, 2, 3, \ldots, \infty)$ with a corresponding frequency shift for different caisson configuration from $kL = n\pi$, which is the asymptotic solution for the gap width $2a \to 0$, as shown in Eq. (A.30) in the Appendix. In the frequency range with engineering interests, the resonant wave number around $n = 1$ and 2 would be important as one may notice in Figs. 2 and 3.

Figure 4 depicts the resonant wave number k detected in the systematic computations for various caisson length L including $\alpha = 0°$ and 90°, together with the dotted curves of $k = n\pi/L(n = 1, 2)$, which is the asymptotic solution for the gap width $2a \to 0$ as shown in Eq. (A.30) for comparison. In this figure, the horizontal axis denotes the length of caisson (gap length) L, and the vertical axis denotes the resonant wave number k, and the non-dimensional wave number kL is expanded up to about 8.0 as the maximum value. And moreover, all of resonant points detected in the systematic computations are shown in the figure. For example, two resonant wave numbers, $k = 1.75$ and $k = 2.8$, for $L = 2$ correspond to the sharp peak responses calculated in Fig. 2, while in the case of $L = 3.0$, three resonant wave numbers have been detected. Then, each resonant wave number is distinguished as $n = 1$ or $n = 2$, according to the approach of kL against the asymptotic solutions

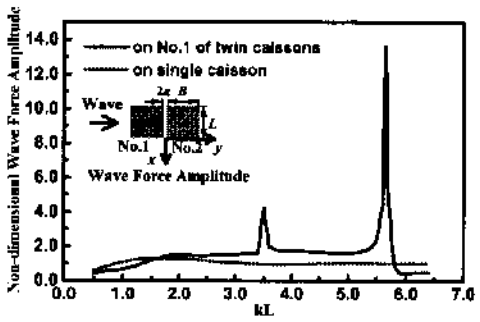

(a) In-line wave force on the No. 1 caisson when $\alpha = 90°$.

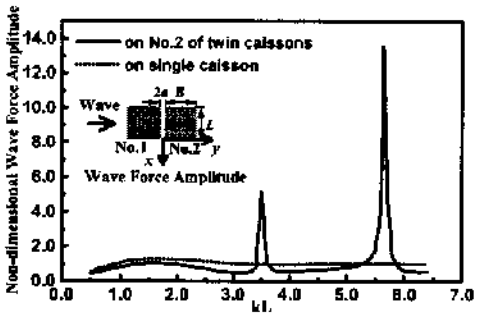

(b) In-line wave force on the No. 2 caisson when $\alpha = 90°$.

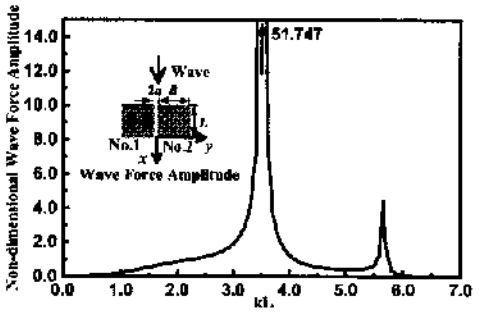

(c) Cross wave direction force on the No. 1 caisson when $\alpha = 0°$.

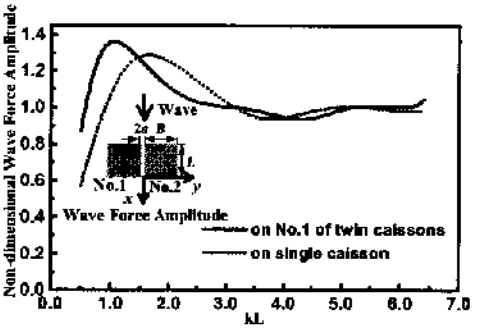

(d) In-line wave force on the No. 1 caisson when $\alpha = 0°$.

Fig. 2. Wave force on twin caissons of $L = 2$.

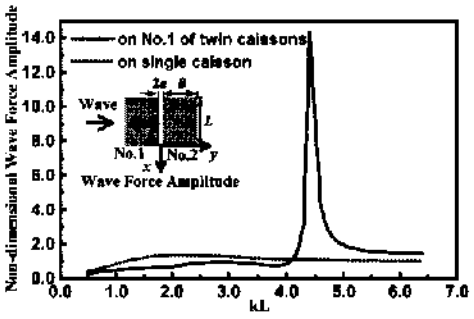

(a) In-line wave force on the No. 1 caisson when $\alpha = 90^{\circ}$.

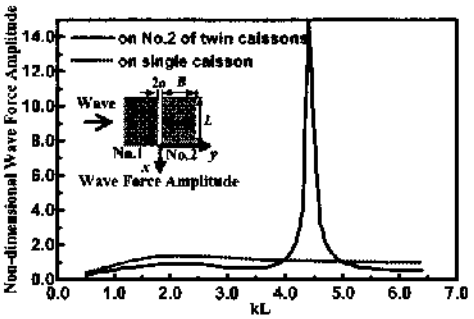

(b) In-line wave force on the No. 2 caisson when $\alpha = 90^{\circ}$.

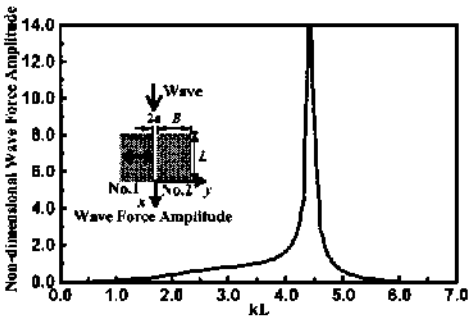

(c) Cross wave direction force on the No. 1 caisson when $\alpha = 0^{\circ}$.

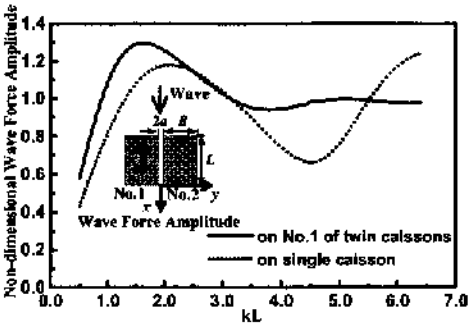

(d) In-line wave force on the twin caissons of $L = 4$.

Fig. 3. Wave force on twin caissons of $L = 4$.

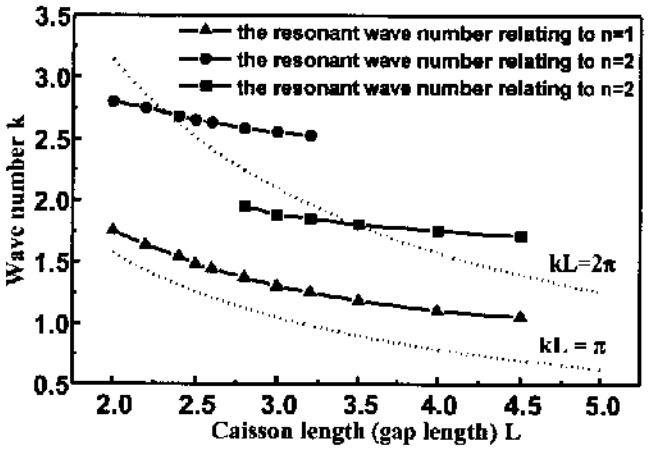

Fig. 4. The resonant wave numbers detected in the computation for different twin caissons.

$n\pi(n = 1, 2)$. As shown from the figure, for the case of $n = 1$, the resonant frequencies will always shift to the higher frequency range. However, the resonant frequency shifts around $n = 2$ exhibit a little bit complex nature. Due to the principal effects of the wave diffraction, the frequency shifts to both higher and lower frequency ranges may appear simultaneously for some caisson configurations, as shown in the figure. Since the motion in the gap is similar to the wave motion in a narrow open channel, such resonant phenomena may be called as the "narrow open channel resonance", because this phenomena is different from the well know harbor resonance which is caused by both closed condition and the condition with one end open. Moreover, this resonant conditions, around $kL = n\pi(n = 1, 2, 3, \ldots, \infty)$, which depend on the gap length L, are different from the trapped mode. It seems that the present investigation is the first time to point out the existence of the narrow open channel resonant phenomena. Forces on each caisson near the resonant frequencies may reach as high as tens of those on the corresponding isolated single caissons. As one may understand from Eq. (A.31), the small yet finite gap width will also give influence on the resonant frequency shift and resonant force amplitude, the results of which will be reported elsewhere.

Besides the resonant phenomena, the hydrodynamic interaction is also clear as noticed from the results. In the shorter wave range, we may see from Figs. 2(a) and (b), 3(a) and (b) that the in-line wave force on the No. 1 caisson is larger than that on a single caisson and on the contrary for the in-line wave force on the No. 2 caisson. It shows that, generally speaking, the shielding effects of the leading caisson will become important in the shorter wave range except the frequency bands near the resonant frequencies. In the longer wave range, however, the in-line wave forces on both the Nos. 1 and 2 caissons are lower than that on a single caisson and no shielding effects can be detected. We may regard that the reduction of the wave forces in the longer wave range is mainly caused by the interference between

caissons, if we use the word "interference" in a narrower sense by excluding the shielding effects.

There is no doubt that viscosity of fluid and possible vortex shedding around corners would cause energy dissipation of the fluid flow and, hence, reduce the severity of resonance. Those effects, however, are usually regarded limiting to local regions for the hydrodynamic interaction problem between waves and structures of large scale, especially for the general properties of the interaction. For the purpose of the present study, inclusion of those effects will give no influence to the essence of the interaction property and resonance.

It is also meaningful to make further comparison of the integrated wave forces on twin caissons, which denotes the summation of wave forces on each caisson according to their phases, with those on the single "two in one" body approximation (as if the gap is also occupied by solid material). Shown in Fig. 5 is the case for the twin caissons with length of 4 as a typical example, from which it is understood

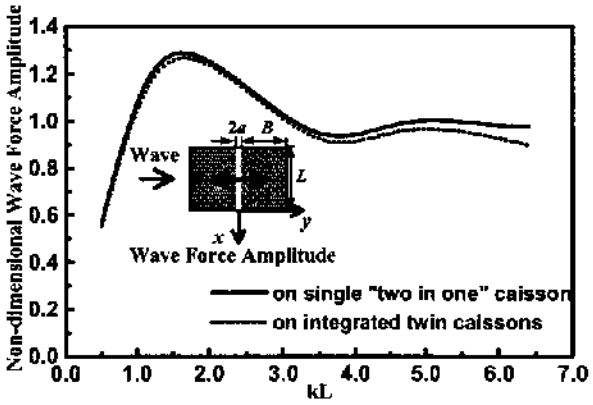

(a) In-line wave forces when $\alpha = 90°$.

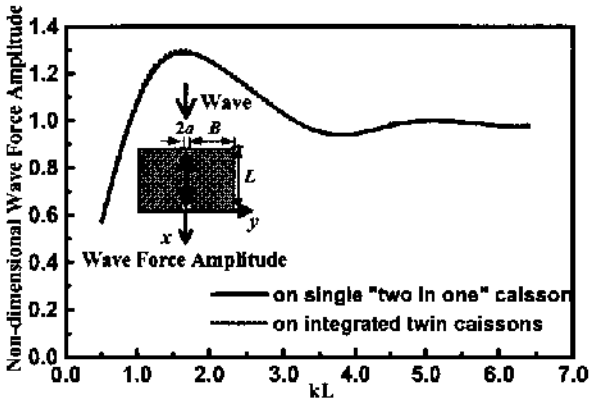

(b) In-line wave forces when $\alpha = 0°$.

Fig. 5. The integrated wave forces on twin caissons with $L = 4$ and $B = 2$ compared with those for corresponding single "two in one" caisson for incident wave angle $\alpha = 0°$ and $90°$.

there is not much difference between them. The importance of strong hydrodynamic interaction feature for multi-bodies is more closely related to the hydro-elasticity analyses for the very large structures, in which local loads may be as important as the integrated loads. And yet, the interaction feature has its own important practical significance for the design of links (connectors) of modules and the attentions on the term of work for linking the modules.

The resonance phenomena are specially recognized for rectangular caissons aligned linearly with small gaps in between. It may become clear if we notice different features of the results for twin circular cylinders of unit radius aligned with the same gap as for twin caissons, as shown in Fig. 6. Figure 6(a) depicts the in-line wave forces in the oy direction when the wave incident angle $\alpha = 90°$ on cylinders Nos. 1 and 2 respectively. And Fig. 6(b) shows both the in-line wave forces and cross wave direction forces on each cylinders for $\alpha = 0°$. To be consistent with previous

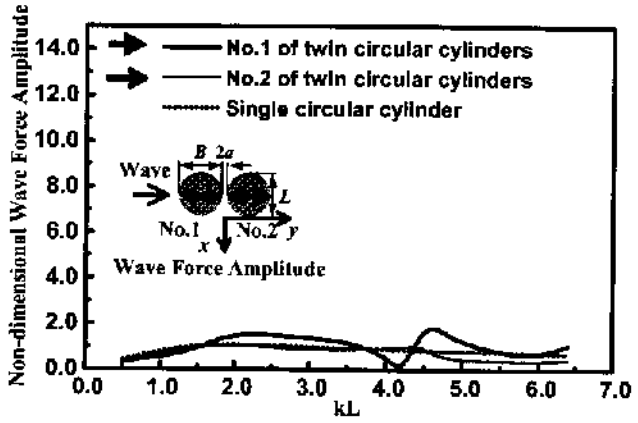

(a) In-line wave forces on twin circular cylinders when $\alpha = 90°$.

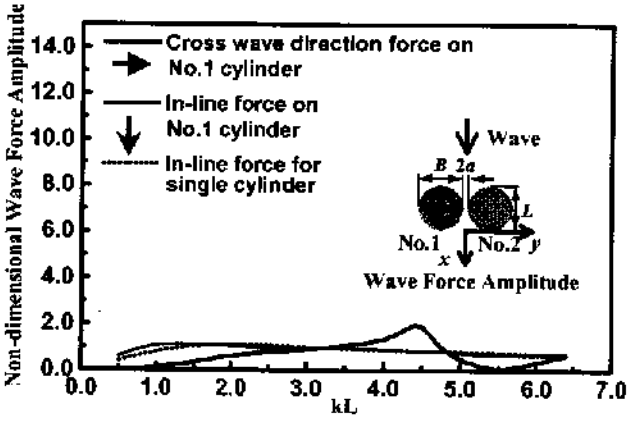

(b) In-line and cross wave direction forces on twin circular cylinders when $\alpha = 0°$.

Fig. 6. Wave forces on twin circular cylinders with the same gap as twin square caissons for wave incident wave angle $\alpha = 0°$ and $90°$.

figures, we use L in Fig. 6 to denote the diameter of the circular cylinder of unit radius, i.e. $L = 2$. As seen in these figures, while the hydrodynamic interaction exists, no resonance can be distinguished. Again, we can see, by comparing the results with the isolated single cylinder shown by dotted line in Fig. 6(a), that in longer waves the interference between cylinders is dominant and in shorter wave range the shielding effects of the leading cylinder become important.

4. Concluding Remarks

A reduced two-dimensional source distribution method is used for systematic computations on the wave interaction of twin caissons with rectangular sections aligned with small gap between in order to get a clear fundamental view of the small gap influence to the force response on potentially very large coastal and marine structures. Although the integrated wave forces on twin caissons do not differ much from those on the corresponding single "two in one" body, strong hydrodynamic interaction between caissons is observed. The sharp peak force response on each caisson is proved in the paper by both numerical evidence and theoretical verification due to the newly discovered narrow open channel resonant phenomena. The resonant wave number is proved around $kL = n\pi (n = 1, 2, 3, \ldots, \infty)$ with a corresponding frequency shift. The present study for twin caissons may also give an insight into the complicated hydrodynamic interaction and resonant behavior of more bodies. Due to the complexity of the phenomena, further experimental study should be strongly encouraged for the deeper understanding on that subject besides the investigations in numerical and theoretical ways.

Limiting to very large floating structures, the resonance presented in this study may become weak. However, care should be made to account for the possible strong interaction between multiple box-shaped bodies. Because the strong hydrodynamic interaction feature has its own important practical significance for the design of links (connectors) of modules for the very large structure and the attentions on the term of work for linking the modules. And the importance is also closely related to the hydro-elasticity analyses of the very large structures, in which local loads may be as important as the integrated loads.

At last, we would like to note that an accurate and yet efficient method for the prediction of the hydrodynamic behavior for the very large structures is still needed for development. The asymptotic matching method mentioned in the Appendix may offer an efficient way to tackle that problem. For a general 3-D very large structure, however, even more efforts should be made.

Acknowledgments

This project is supported by the National Natural Science Foundation of China (Nos. 59879011 and 19732004) and the Foundation of the Ministry of Education of China.

Appendix A. The Mechanism of the New Narrow Open Channel Resonance Phenomena

We will give the mechanism of the resonant phenomena relating to the twin caisson hydrodynamic interaction. The main idea follows the asymptotic matching process used by Mei (1989) for narrow harbor resonance.

Being consistent with the method and the body configuration we adopt, it is only necessary for us to consider the corresponding reduces two-dimensional problem (the variation in the water depth direction is separated as $\cosh k(z+h)/\cosh kh$ by using the method of separation of variables, as we mentioned above).

As shown in Fig. A.1 for the plane view of twin caissons, we may divide the whole fluid domain into following four regions: (1) the outer far field around all the bodies, (2) two near fields around both the gap ends at $x = 0$ and $x = -L$, and (3) the inner far field (the fluid region in the gap away from two gap ends). We will indicate the variables relating to the gap ends at $x = 0$ and $x = -L$ with subscripts R and L, respectively.

In the outer far field, the details of the gap can no longer be detected. The influence of the gap can be regarded as two pulsating sources at the locations P_R and P_L of the gap ends on the wall of a single "two in one" body as if the two bodies were attached together, as shown in Fig. A.2.

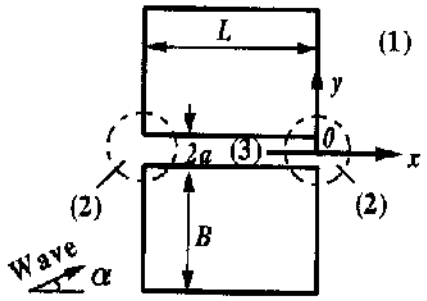

Fig. A.1. A sketch for the definition of fluid regions.

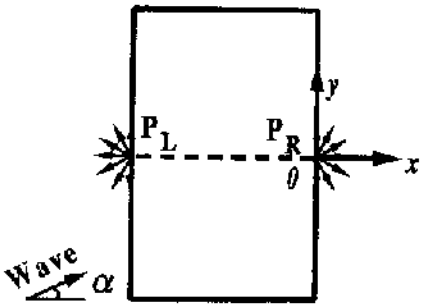

Fig. A.2. Approximation of flow in the outer far field.

The total velocity potential $\phi_0(x, y)$ at any field point in the outer far field may be written as

$$\phi_0 = \phi_I + \phi_D + \phi_S \tag{A.1}$$

ϕ_I is the incident wave potential given in Eq. (2). ϕ_D is the diffraction potential, which can be represented by the source and sink distribution method as

$$\phi_D = \frac{1}{4\pi} \int_C \sigma(Q) G(P, Q) dl \,. \tag{A.2}$$

Although Eq. (A.2) has the same expression as Eq. (8) with the same fundamental source as Eq. (9), two main differences should be noticed. One is that the girth C here denotes the outer girth of the single "two in one" caisson as if they joined together. And the other is that to determine the source distribution strength $\sigma(Q)$, not only the incident wave potential but also the influence of two extra sources simulating the existence of the gap should be taken into account. The potential caused by those two extra sources may be expressed as

$$\phi_S = Q_R H_0^{(1)}(kr_R) + Q_L H_0^{(1)}(kr_L) \tag{A.3}$$

where $H_0^{(1)}(kr_{R(L)})$ is the first kind Hankel function of the zero-th order satisfying the radiation condition of out-going disturbance waves, r_R, r_L represent the distances of the field point $P(x, y)$ to the right-hand and left-hand source points, at which the sources have their strengths of Q_R and Q_L, respectively.

The relationship between source strengths of $\sigma(Q)$, Q_R and Q_L can be determined by imposing the body surface condition as we do for Eq. (13), which becomes

$$[E]\{\sigma\} + \{D_R\}Q_R + \{D_L\}Q_L = \{F\} \tag{A.4}$$

in which the influence matrix$[E]$ has its elements as shown in (12) and $\{F\}$ has its elements shown as the right-hand term of Eq. (10). Notice that the body girth C now does not include the boundaries in the gap. $\{D_R\}$ and $\{D_L\}$ have elements as

$$\frac{\partial H_0^{(1)}(kr_{R(L)}(P_i))}{\partial n}, \qquad i = 1, 2, \ldots, N \tag{A.5}$$

respectively, denoting the normal velocity induced at each point P_i on the outer body girth by the extra sources at both the gap ends. Then, the relationship between source strengths of $\sigma(Q)$, Q_R and Q_L can be expressed as

$$\{\sigma\} = -[E]^{-1}\{D_R\}Q_R - [E]^{-1}\{D_L\}Q_L + [E]^{-1}\{F\} \,. \tag{A.6}$$

To actually solve Eq. (A.4), two extra conditions are needed, which will be offered by the matching process.

With the above relationship, the diffraction potential ϕ_D at any point P in the fluid domain can be determined by Eq. (8), the discretized form of which may also be written in a matrix expression as

$$\begin{aligned}\phi_D(P) &= \{T\}^T\{\sigma\} \\ &= -\{T\}^T[E]^{-1}\{D_R\}Q_R - \{T\}^T[E]^{-1}\{D_L\}Q_L + \{T\}^T[E]^{-1}\{F\}\end{aligned} \tag{A.7}$$

where

$$T_j = \frac{1}{4\pi}\int_{\Delta C_j} G(P,Q_j)dl\,. \tag{A.8}$$

Again, ΔC_j are the divided linear segments of the outer girth of the single "two in one" caisson. The inner expansion of the outer solution ϕ_0 when P tends to P_R and P_L becomes

$$\begin{aligned}\phi_o|_{P\to P_R} &= \bar{A} - \{T_R\}^T[E]^{-1}\{D_R\}Q_R - \{T_R\}^T[E]^{-1}\{D_L\}Q_L + \{T_R\}^T[E]^{-1}\{F\} \\ &\quad + \left(1 + \frac{2i}{\pi}\ln\frac{\gamma k r_R}{2}\right)Q_R + H_0^{(1)}(kL)Q_L\end{aligned} \tag{A.9}$$

$$\begin{aligned}\phi_o|_{P\to P_L} &= \bar{A}e^{-ikL\cos\alpha} - \{T_L\}^T[E]^{-1}\{D_R\}Q_R - \{T_L\}^T[E]^{-1}\{D_L\}Q_L \\ &\quad + \{T_R\}^T[E]^{-1}\{F\} + H_0^{(1)}(kL)Q_R - \left(1 + \frac{2i}{\pi}\ln\frac{\gamma k r_L}{2}\right)Q_L\end{aligned} \tag{A.10}$$

in which $\ln\gamma$ = Euler's constant = $0.5772157\ldots$, $\{T_{R(L)}\}^T$ has the elements as shown in (A.8) but with P changed to P_R or P_L, and r_R and r_L denote the distances of a field point to P_R and P_L, respectively.

For the near field solution around the gap ends where the length scale is the gap width, the governing equation can be reduced to the 2-D Laplace equation with a relative error of order $O(ka)^2$. Solutions around each end of gap may be obtained by the Schwarz-Christoffel transformation as shown in Fig. A.3 (Mei, 1989). For the right-hand end of the gap, the transformation relation will be

$$z = \frac{2a}{\pi}\left[-j(\tau^2-1)^{1/2} + \ln\frac{\tau}{(\tau^2-1)^{1/2}+j}\right] \qquad z = x + jy,\quad j = \sqrt{-1} \tag{A.11}$$

which maps the physical inner region around the gap end of $x = 0$ shown in Fig. A.1 onto the upper half of the τ plane. The velocity potential in the τ plane will be the real part (denoted by Re_j) of the complex potential $W(\tau)$, i.e.

$$\phi = \mathrm{Re}_j W(\tau) = \mathrm{Re}_j(M\ln\tau + C)\,. \tag{A.12}$$

The coefficients M and C are real with respect to j and will be determined by matching process. Its outer expansions will be as follows for different sides, i.e. on

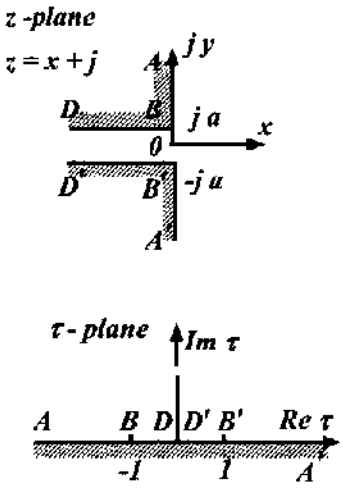

Fig. A.3. Mapping of the region around gap end from the z plane to the upper half of the τ plane.

the gap side where $x < 0$, large $|z|/a$ corresponds to small $|\tau|$ and the expansion of (A.11) becomes

$$\begin{aligned} \frac{\pi z}{2a} &= 1 + \ln\tau - \ln 2j + O(\tau^2) = \ln\frac{e\tau}{2j} + O(\tau^2) \\ \tau &= \frac{2j}{e} e^{\frac{\pi z}{2a}} \quad \text{and} \quad \ln\tau = \frac{\pi z}{2a} - \ln\frac{e}{2j}. \end{aligned} \tag{A.13}$$

Substituting it into (A.12), the outer expansion of the inner solution will be

$$\phi \sim \mathrm{Re}_j\left(M\left[\frac{\pi z}{2a} - \ln\frac{e}{2j}\right] + C\right) = M\frac{\pi x}{2a} - M\ln\frac{e}{2} + C \qquad \text{for } x < 0 \tag{A.14}$$

And on the sea side where $x > 0$, large $|z|/a$ corresponds to large $|\tau|$ and the expansion of (A.11) for $|\tau| \to \infty$ becomes

$$z = \frac{2a}{\pi}\left[-j\tau + O\left(\frac{1}{\tau}\right)\right], \qquad -j\tau = \frac{\pi z}{2a}\left[1 + O\left(\frac{a}{z}\right)^2\right] \qquad \text{for } x > 0.$$

Substituting it into (A.12), the outer expansion of the inner solution will be

$$\phi \sim \mathrm{Re}_j\left(M\ln\frac{j\pi z}{2a} - C\right) = M\ln\frac{\pi r}{2a} - C. \tag{A.15}$$

The inner solution and its outer expansion around the left-hand end of the gap can be obtained in a similar way by translating the coordinate system from $x = 0$ to $x = -L$ and rotating for 180°. The expressions of the inner solution and its outer expansion around the left-hand end of the gap are then the same as those for the right-hand gap end, but with different coefficients, denoted as $\bar{M}$ and $\bar{C}$ hereinafter, respectively.

For the solution in the inner far field, the variation in y-direction may be disregarded since the gap width is small compared with the main dimensions of caissons. Indeed, the inclusion of any variation in y-direction would give influence in the higher frequency range out of practical significance. A general solution of the velocity potential $\phi_g(x)$ in the inner far field may then be written as

$$\phi_g = Be^{-ikx} + De^{ikx} \qquad \text{in the gap} \tag{A.16}$$

with the inner expansion at $x = 0$ and $x = -L$, respectively, as

$$\phi_g|_{x\to 0} = (B + D) + ik(-B + D)x + \cdots + O(kx)^2 \tag{A.17}$$

$$\phi_g|_{x\to -L} = (Be^{ikL} + De^{-ikL}) + ik(-Be^{ikL} + De^{ikL})(x + L) + \cdots + O(k(x + L))^2 . \tag{A.18}$$

Matching of (A.9) with (A.15) and (A.17) with (A.14) for the right-hand gap end gives the following relations, i.e.

$$B + D = C - M \ln \frac{e}{2} \tag{A.19}$$

$$ik(-B + D) = \frac{\pi M}{2a} \tag{A.20}$$

$$A_R + R_R Q_R + H_R Q_L = C + M \ln \frac{\pi}{2a} \tag{A.21}$$

$$\frac{2i}{\pi} Q_R = M . \tag{A.22}$$

For simplicity, use has been made of the following notations in (A.21), i.e.

$$1 + \frac{2i}{\pi} \ln \frac{\gamma k}{2} - \begin{cases} \{T_R\}^T [E]^{-1} \{D_R\} \\ \{T_L\}^T [E]^{-1} \{D_L\} \end{cases} = \begin{cases} R_R \\ R_L \end{cases}$$

$$H_0^{(1)}(kL) - \begin{cases} \{T_R\}^T [E]^{-1} \{D_L\} \\ \{T_L\}^T [E]^{-1} \{D_R\} \end{cases} = \begin{cases} H_R \\ H_L \end{cases}$$

$$\bar{A} + \{T_R\}^T [E]^{-1} \{F\} = A_R$$

$$\bar{A} e^{-ikL\cos\alpha} + \{T_L\}^T [E]^{-1} \{F\} = A_L .$$

Similar matching of (A.10) and (A.18) (after making coordinate system translation and rotation) with the outer expansions of the near field solution of the left-hand gap end will give the relations as

$$Be^{ikL} + De^{-ikL} = \bar{C} - M \ln \frac{e}{2} \tag{A.23}$$

$$ik(Be^{ikL} - De^{-ikL}) = \frac{\pi \bar{M}}{2a} \tag{A.24}$$

$$A_L + H_L Q_R + R_L Q_L = \bar{C} + \bar{M} \ln \frac{\pi}{2a} \tag{A.25}$$

$$\frac{2i}{\pi} Q_L = \bar{M} \,. \tag{A.26}$$

Equations (A.19)–(A.26) together with Eq. (A.4) form the complete set of equations to determine all the coefficients and source strengths. Since the present purpose for us is to exhibit the resonant phenomena, we do not try to really solve the set numerically, which will leave as later investigation. After some fundamental derivations for Eqs. (A.19)–(A.26), the following two equations can be obtained, i.e.

$$[(1 + ka\hat{R}_R) - kaH_R e^{ikL}]B + [(1 - ka\hat{R}_R) + kaH_R e^{-ikL}]D = A_R \tag{A.27}$$

$$[(1 - ka\hat{R}_L)e^{ikL} + kaH_L]B + [(1 + ka\hat{R}_L)e^{-ikL} - kaH_L]D = A_L \tag{A.28}$$

where

$$\left.\begin{matrix} \hat{R}_R \\ \hat{R}_L \end{matrix}\right\} = \left\{\begin{matrix} R_R \\ R_L \end{matrix}\right. + \frac{2i}{\pi} \ln \frac{4a}{e\pi} = 1 + \frac{2i}{\pi} \ln \frac{2\gamma ka}{e\pi} - \left\{\begin{matrix} \{T_R\}^T [E]^{-1} \{D_R\} \\ \{T_L\}^T [E]^{-1} \{D_L\} \,. \end{matrix}\right.$$

The resonance will happen when the coefficient determinant of Eqs. (A.27) and (A.28) equals zero, which means that the amplitude in the inner far field will be infinity, i.e. when

$$[1 + (ka)^2(\hat{R}_R \hat{R}_L - H_R H_L)] \sin kL + ika(\hat{R}_R + \hat{R}_L) \cos kL - ika(H_R + H_L) = 0 \,.$$

Since the second and third terms will vanish as ka really tends to zero, the first term gives the possible resonant wave numbers, which are

$$\sin kL = 0 \quad \text{and} \quad kL = n\pi, \quad n = 1, 2, \ldots \tag{A.29}$$

For small but finite ka, the response peak will happen near the roots of the equation

$$\begin{aligned} &[1 + (ka)^2 \mathrm{Re}(\hat{R}_R \hat{R}_L - H_R H_L)] \sin kL \\ &\quad - ka \,\mathrm{Im}(\hat{R}_R + \hat{R}_L) \cos kL + ka \,\mathrm{Im}(H_R + H_L) = 0 \end{aligned} \tag{A.30}$$

where Re and Im denote the real and imaginary parts of a complex variable, respectively. The roots of the equation for kL will near $n\pi$ but with a certain frequency shift.

The existence of the new narrow open channel resonance is thus proved.

References

Dalrymple, R. A. and Martin, P. A. (1990). Wave diffraction through offshore breakwater, *J. Waterway, Port Coast. Ocean Eng.*, ASCE **116-6**: 727–741.

Evans, D. V. and Porter, R. (1997). Trapped modes about multiple cylinders in a channel, *J. Fluid Mech.* **339**: 331–356.

Fernyhough, M. and Evans, D. V. (1995). Scattering by a periodic array of rectangular blocks, *J. Fluid Mech.* **305**: 263–279.

Isaacson, M. (1978). Vertical cylinders of arbitrary section in waves, *J. Waterway Port Coast. Ocean Div.*, ASCE **104-4**: 309–324.

Kagemoto, H., Fujino, M. and Zhu, T. (1997). On the estimation method of hydrodynamic forces acting on a very large floating structure, *Appl. Ocean Res.* **19**: 49–60.

Kim, M. H. (1993). Interaction of waves with N vertical circular cylinders, *J. Waterway Port Coast. Ocean Eng.*, ASCE **119-6**: 671–689.

Kiyokawa, T. and Motyka, V. (1990). Green function for analyzing scattering of water wave by an infinitely periodic row of cylinders and its applications, *Tech. Res. Rep. Shimizu Corp.* **52**: 53–63.

Linton, C. M. and Evans, D. V. (1990). The interaction of waves with an array of circular cylinders, *J. Fluid Mech.* **215**: 549–569.

Mei, C. C. (1989). *The Applied Dynamics of Ocean Surface Waves*, World Scientific, Singapore, pp. 199–206.

Miao, G. P. and Liu, Y. Z. (1990). Hydrodynamic forces for large vertical cylinders of arbitrary section, *China Ocean Eng.* **4-2**: 145–158.

Miao, G. P., Liu, Y. Z. and Mi, Z. X. (1993). Computation of hydrodynamic forces on vibrating multiple large vertical cylinders of arbitrary section, *Marine Structures* **6**: 279–294.

Miao, G. P., Yu, Z. X., Miao, Q. M., Liu, Y. Z. and Zhang, H. X. (1998). On hydrodynamics interaction upon the wave forces on vertical pile array, *J. Hydrodyn.* **B-3**: 69–79.

Nakamura, T. (1994). Wave directional change by an array of breakwaters, *Proc. Waves Phys. Numer. Model.*, pp. 1069–1078.

Nakamura, T. (1997). Wave interactions with an infinite arrary of 3-D bodies, *Proc. 7th Int. Offshore Polar Eng. Conf.* **III**: 524–528.

Ohkusu, M. (1976). Ship motions in vicinity of a structure, *Proc. BOSS'76*, pp. 284–306.

Oortmerssen, G. V. (1979). Hydrodynamic interaction between two structures floating in waves, *Proc. BOSS'79*, pp. 339–356.

Yu, Z. X., Miao, G. P. and Liu, Y. Z. (1998). On the effects of hydrodynamic interaction upon the wave forces on pile arrays of multiple rows, *Proc. 8th Int. Offshore Polar Eng. Conf.* **III**: 513–518.